



Laboratory Observation of Radiative Shock Deceleration and Application to SN 1987A

Th. Michel¹, B. Albertazzi¹, P. Mabey¹, G. Rigon¹, F. Lefevre¹, L. Van Box Som², P. Barroso³, S. Egashira⁴, R. Kumar⁴, C. Michaut⁵, M. Ota⁴, N. Ozaki^{4,6}, Y. Sakawa⁴, T. Sano⁴ , E. Falize², and M. Koenig^{1,6}

¹ LULI-CNRS, Sorbonne Universités, Ecole Polytechnique, Institut Polytechnique de Paris, F-91128 Palaiseau Cedex, France; b.albertazzi@hotmail.fr

² CEA, DAM, DIF, F-91297 Arpajon, France

³ GEPI, Observatoire de Paris, PSL Research University, CNRS, 61 Avenue de l'Observatoire, F-75014 Paris, France

⁴ Institute of Laser Engineering, Osaka University, Suita, Osaka 565-0871, Japan

⁵ Université Côte d'Azur, Observatoire de la Côte d'Azur, CNRS, Laboratoire Lagrange, Bd de l'Observatoire, CS 34229, 06304 Nice cedex 4, France

⁶ Graduate School of Engineering, Osaka University, Osaka, 565-0871, Japan

Received 2019 September 10; revised 2019 November 15; accepted 2019 November 18; published 2019 December 31

Abstract

The first laboratory evidence of a radiative shock (RS) decelerating during its free expansion phase in an optically thick medium is presented. A shock is generated in a multilayer solid target under the irradiation of a high-power laser at the GEKKO XII laser facility. The rear surface of the target is connected to a gas cell filled with Xe. Upon breakout, an RS, characterized by low Boltzmann number $Bo \ll 1$ and Mihalas number $R \approx 10$, is generated. Experimental results reveal that radiative losses through the radiative precursor cause the shock to lose energy and decelerate. A model is developed that describes the shock propagation as a function of time. The model is in agreement with both numerical simulations and experimental results. These results have tremendous consequences for astrophysical systems, such as SN 1987A, where radiative deceleration may play a role in the formation of the observed hotspots in the circumstellar ring.

Unified Astronomy Thesaurus concepts: [Laboratory astrophysics \(2004\)](#); [Experimental techniques \(2078\)](#); [Shocks \(2086\)](#)

1. Introduction

Radiative shock (RS) waves can be found in many astrophysical systems, such as supernova explosions, young stellar objects (Orlando et al. 2013), cataclysmic variables (Busschaert et al. 2015; Van Box Som et al. 2018), accretion disks and accreting neutron stars (Shapiro & Salpeter 1975). These violent phenomena inject energy into the interstellar medium, strongly influencing its dynamics. For example, the interaction between shocks and interstellar objects, such as molecular clouds, is thought to be a possible trigger mechanism for star formation, which itself is important for understanding galaxy dynamics (Nagakura et al. 2009).

In most astrophysical shocks, the temperature and density conditions lead to strong emission, and thus radiation plays a major role. RSs are often divided into two classes depending on whether the shocked medium is optically thin or thick. We will focus our attention here on the case where the medium is optically thick, i.e., radiation is absorbed by the upstream region. This leads to the generation of a heated zone in front of the shock front, usually referred to as a “radiative precursor.” This region is of particular interest because it plays a role in the equation for the energy balance of the system (Drake 2007).

RSs and their precursors are generated when supernova remnants interact with the circumstellar medium (Chevalier 1982; Ensmann & Burrows 1992; Staveley-Smith et al. 1993; Lawrence et al. 2000). However, supernova explosions are very difficult to model numerically because of the different spatial and temporal length scales involved (Orlando et al. 2015). Direct astronomical observation is also difficult, because the downstream region often becomes optically thick to its own radiation, preventing it from escaping the system. It is therefore essential to study the propagation of RSs in an optically thick medium, in the laboratory, in order to fully understand the physics underpinning such shocks.

Many laboratory studies on radiative blast waves have already been performed (Edwards et al. 2001; Hansen et al. 2006), which demonstrate the importance of radiation for the dynamics of the system. Studies on radiative effects in planar shock waves have also been carried out (Doss et al. 2009; Bouquet et al. 2011; Drake et al. 2011; Suzuki-Vidal et al. 2011), including the characterization of a radiative precursor (Vinci et al. 2006), and they highlight the importance of avoiding preheating of the ambient gas in which the shock propagates (Koenig et al. 2017). However, there is not yet any experimental evidence of the deceleration of an RS during its free expansion phase (i.e., when the mass swept up by the wave is less than the mass of the wave).

In this article, we present experimental results on a freely expanding shock, in an optically thick, high-Z, low-density gas, decelerating only as a result of radiative losses. A self-consistent analytical model is presented that does not assume a constant shock velocity and takes into account the radiation absorbed in the precursor. The observed deceleration is in agreement with the experimental results and numerical simulations. We are thus able to gain a new insight into the hotspot formation in the circumstellar medium around Type II supernovae such as SN 1987A, which are currently only partially understood (Müller et al. 1991).

2. Experimental Setup

We use the GEKKO XII laser facility (Osaka, Japan) to produce an RS, with a full description of the experimental platform available in Michel et al. (2018). We use nine beams at a wavelength of 351 nm. The total energy on target is 1200 J, the focal spot is 350 μm in diameter, and the pulse duration is 500 ps. The beams are focused onto a solid multilayer target made of an ablator (10 μm polystyrene (CH)) and a shield (1.5 μm Au/6 μm Ti) to prevent preheating. This

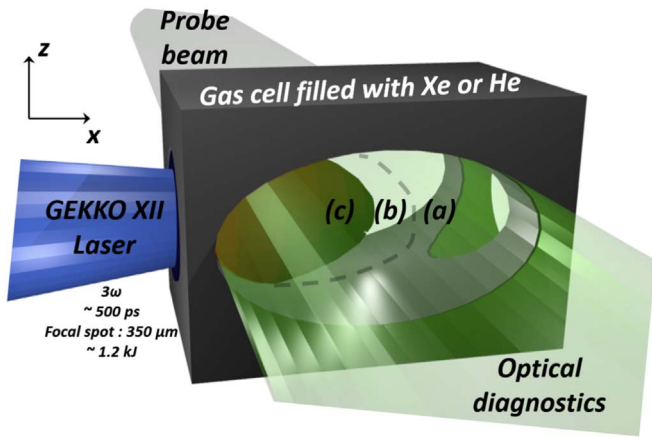


Figure 1. Experimental setup used at GEKKO XII and morphology of the radiative shock created in an optically thick medium, where (a) is the propagating medium (initially at rest), (b) is the radiative precursor, and (c) is the downstream region. The cell is filled with gas (Xe or He).

creates a shock that propagates in a gas cell (see Figure 1). To quantify radiative effects in the laboratory, two dimensionless numbers are introduced: the Mihalas number R , the ratio between the thermal energy density and the radiative energy density, and the Boltzmann number Bo , the ratio between the enthalpy flux and the radiative flux (Drake 2005; Michaut et al. 2009). High- Z , low-density gases favor stronger radiative effects (i.e., lower Bo and R). The gas cell is therefore filled with 31 mbar of xenon (high Z) or 1 bar of helium (low Z) in order to observe the system with and without radiative effects (i.e., the presence of a radiative precursor), while keeping the mass density constant.

Two optical diagnostics are implemented to measure relevant parameters of the shock: time-resolved interferometry to obtain the electron density in the upstream region at a given time, and streaked shadowgraphy to track the position of the shock front as a function of time.

3. Results

Figure 2 shows an interferometry image and its associated electron density map retrieved from Abel inversion for xenon gas at a given time. Region (a) corresponds to the unperturbed medium in which the shock propagates. The radiative precursor (region (b)) is clearly identified; it has a length of $600 \mu\text{m}$ with a smooth density profile from $5 \times 10^{19} \text{cm}^{-3}$ to the initial ion density (a few 10^{18}cm^{-3}) of the Xe gas. Finally, region (c) corresponds to the downstream region, which appears opaque to visible light due to its electron density being above the critical density (defined as $n_e [\text{cm}^{-3}] \approx 1.11 \times 10^{21} / \lambda^2$ where λ is the wavelength of the probe beam, here 532nm). This is the typical morphology of an RS with a low Bo .

Figure 3 shows a streaked shadowgraphy image of the shock propagating in xenon and helium at the same mass density and for a high initial velocity of $\sim 150 \text{km s}^{-1}$. This shows the limit between where the probe laser light is absorbed and where it is not absorbed (which corresponds here to an electron density of $n_e \approx 3.9 \times 10^{21} \text{cm}^{-3}$). The shock front is clearly visible and corresponds to the threshold between the opaque (to the laser probe) downstream region (c) and the transmissive upstream regions (a) and (b). No significant difference in light absorption exists between these two regions, mainly because the electron density is too low in the precursor compared to the critical

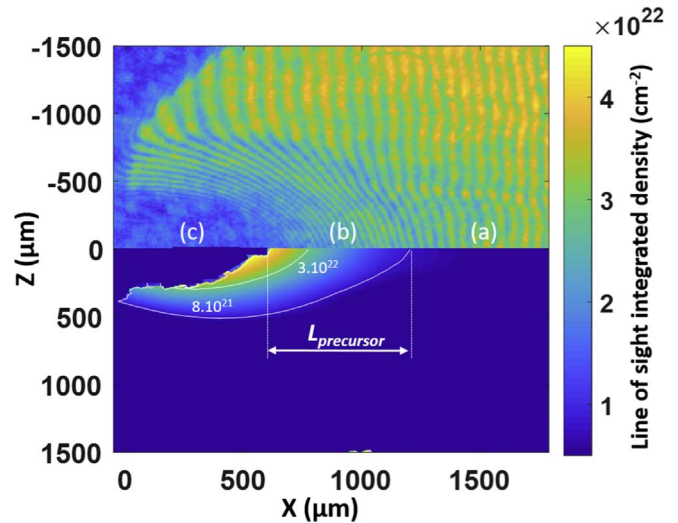


Figure 2. Interferometry image of a radiative shock propagating in xenon (31 mbar), 8 ns after the drive beam. The upper half shows the raw data, while the lower half shows the electron density map after analysis. Regions (a)–(c) are indicated in Figure 1.

density. The position of the shock front is measured explicitly by taking various horizontal lineouts, each corresponding to a 1D snapshot in time, and then determining the midpoint of the change of intensity around the shock front. One therefore arrives at the distance traveled by the shock front as a function of time. The error bar regarding the shock position using this method is $\sim 15 \mu\text{m}$.

The two images exhibit a different morphology (curved line for xenon, straight line for helium) that is quantified below. In the helium case, the slope is constant, implying a constant shock velocity. This is in contrast to the Xe case, where the slope is not constant over time, highlighting a deceleration of the shock. Due to the otherwise identical nature of the two systems, we conclude that this deceleration is due to the stronger radiative effects present in xenon. These results therefore represent the first laboratory observation of a shock decelerating solely due to radiation. The data presented here agree qualitatively with previous studies using cluster targets (Hohenberger et al. 2010) (i.e., the emission of radiation causes a deceleration of the shock). However, the differences in experimental conditions prevent a direct quantitative comparison.

4. Analytical Model

In support of this conclusion, and in order to apply these results to astrophysical systems, we now quantify the energy losses of the shock leading to its deceleration. Many studies on laser-produced plasmas and astrophysical systems assume the shock velocity to be constant and the upstream medium optically thin, thus allowing the use of a cooling function and the energy balance equation to estimate the energy losses in the system (Pun et al. 2002; Hohenberger et al. 2010). However, this method cannot explain the rate of deceleration of the shock. Moreover it is not applicable universally, namely when the upstream region is not transparent to the emitted radiation. This is the case in numerous astrophysical systems, such as SN 1987A, and in our system. In an optically thick region, losses are due to radiation of the shock front through the radiative

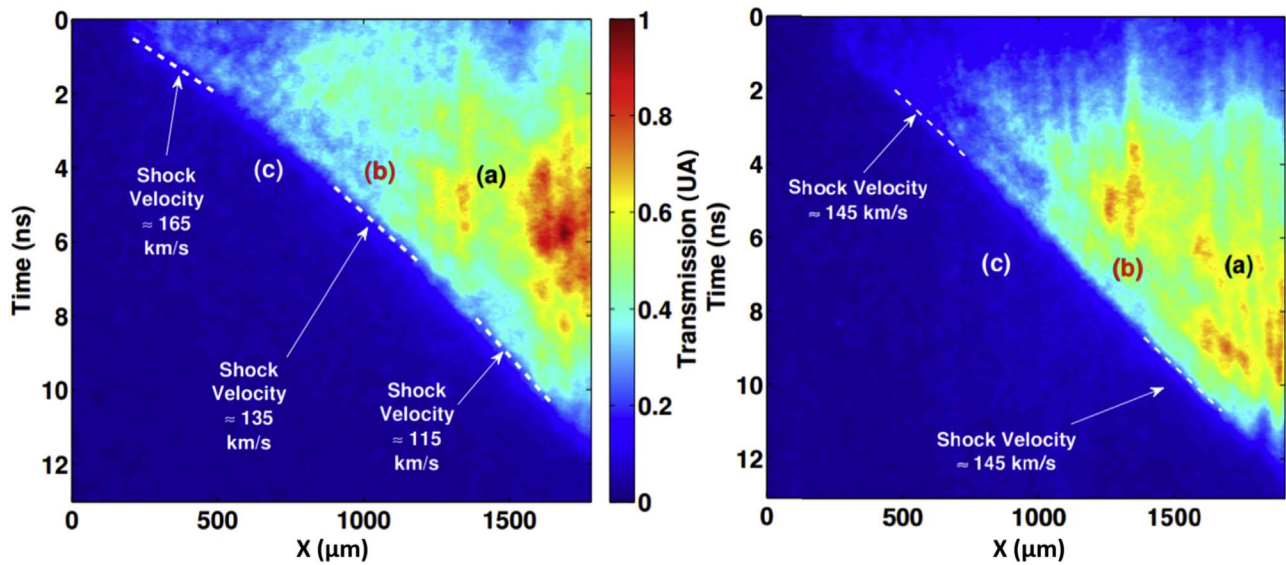


Figure 3. Streaked shadowgraphy images of the shock propagating in xenon (left) and helium (right). Both display high initial velocities but deviate at later times, with the shock front decelerating in xenon but maintaining a constant speed in helium.

precursor region. We therefore present an alternative, self-consistent analysis.

The radiative power losses per unit volume can be expressed as $\nabla \cdot \mathbf{F}_{\text{rad}}$, where \mathbf{F}_{rad} is the radiative flux. Hence, the radiative flux is related to the radiative energy E_{rad} by

$$|\mathbf{F}_{\text{rad}}| = \frac{-\lambda_R}{3} c \frac{\partial E_{\text{rad}}}{\partial x} \approx \frac{c \lambda_R E_{\text{rad}}}{3L} \quad (1)$$

where L is the gradient length defined by $\nabla \cdot \mathbf{F}_{\text{rad}} \approx F_{\text{rad}}/L$, λ_R is the Rosseland mean free path, and c is the speed of light (Zel'dovich & Raizer 2002). L corresponds to the radiative precursor length and is directly measured experimentally.

As we are considering radiative fluxes, it would intuitively be more relevant to use the Boltzmann number Bo to consider radiative losses rather than the Mihalas number R . However, because the model uses an energy balance regarding the shock, R is used in the following discussion. We first note that the Mihalas number R , which depends on the temperature, the density, and the nature of the gas, can be written as $E_{\text{rad}} = E_{\text{tot}}/(R + 1)$. For high shock velocities (around 150 km s^{-1}) in xenon at 31 mbar, R decreases to approximately 10. This implies that E_{rad} is of the order of 10% of the total energy, enough to modify the dynamics of the shock.

One also notes that R varies with the total energy and consequently with the temperature. Indeed, $E_{\text{rad}} \propto T^4$ and $E_{\text{th}} \propto T$ where E_{th} is the thermal energy, while Bo and R depend on the shock temperature as T^{-3} . This dependence remains true even if the shock is non-stationary, assuming the deceleration is slow enough to maintain a temporal equilibrium near the shock, thus keeping the Rankine–Hugoniot conditions fulfilled on a short timescale. The temperature in the system here is between 17 and 25 eV.

By considering the variation of the Mihalas number with the total energy, and taking into account energy losses through the radiative precursor shown in Equation (1), the partial differential equation for the energy is

$$\frac{dE_{\text{tot}}}{dt} + \frac{c \lambda_R}{3(R_0 + 1)E_0^3 L^2} E_{\text{tot}}(t)^4 = 0, \quad (2)$$

where E_0 and R_0 are the initial total energy and the initial Mihalas number respectively. After manipulation the solution becomes

$$E_{\text{tot}}(t) = E_0 \left[1 + \frac{\lambda_R c}{(R_0 + 1)L^2} t \right]^{-1/3}. \quad (3)$$

The shock velocity, u_s , varies as the square root of the energy, so one obtains

$$u_s(t) = u_0 (1 + t/t_c)^{-1/6}, \quad (4)$$

where u_0 is the initial shock velocity and $t_c = (R_0 + 1)L^2/(\lambda_R c)$ is the characteristic time of radiation diffusion.

One notes that the shock velocity decreases, as expected in a system with energy losses. Moreover, the more radiative the shock is, the faster it decelerates, because R_0 decreases as t_c decreases. As both R_0 and L are much smaller in the xenon case than in the helium one, the deceleration is visible in xenon but not in helium. We note here that the Mihalas number is calculated throughout this paper using the modified Rankine–Hugoniot equations including ionization and radiation together with experimental data inputs.

5. Numerical Simulation

Numerical simulations are also performed in order to check the validity of our model. We use the CEA laser radiation hydrodynamic code FCI2 (Schurtz et al. 2000) with the multi-group diffusion model (300 groups), which is able to accurately reproduce this regime. The simulations are 1.5D, that is to say the hydrodynamics is treated one-dimensionally but the radiative transfer is treated in two dimensions. This method gives an accurate simulated shock temperature, as we checked by comparing it with full 2D simulations. One can also retrieve the shock position in the simulations by tracking the pressure and mass density discontinuity. The distance traveled by the shock according to our model is obtained by simple integration of Equation (4). This requires the knowledge of various parameters (R_0 , L , u_0). L and u_0 are directly measured experimentally while R_0 is determined from the temperature given by FCI2 and the

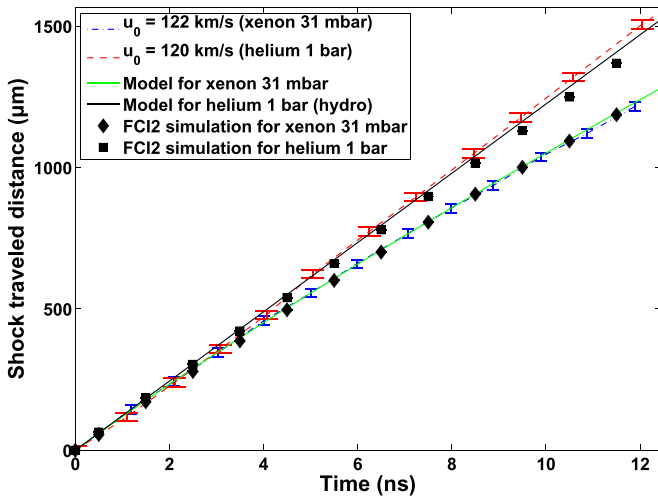


Figure 4. Distance traveled by the shock as a function of time for experiment, simulation, and analytical modeling ($u_0 = 122 \text{ km s}^{-1}$, $R_0 = 15$, $\lambda_R \approx 5 \mu\text{m}$, and $L = 600 \mu\text{m}$, the precursor length).

initial conditions in the gas cell. For the experimental data, the shock position is determined as a function of time, as mentioned previously. The shock position is shown only every nanosecond for the sake of clarity. Initial and final velocity are calculated over an average of 1 ns to have acceptable error bars for the shock velocity.

The comparison between the numerical simulations, the analytical model, and the experimental data for the cases of helium and xenon is shown in Figure 4. Here we used shots where initial velocities are similar (122 km s^{-1} in Xe and 120 km s^{-1} in He, see Table 1). One notes that the model for helium predicts a constant velocity, which is the assumption made in most of the literature on RSs (see, e.g., Drake et al. 2011 and references therein).

It is clear that the RS tends to decelerate in every case (experiment, simulation, analytical model) where a radiative precursor is visible. Moreover, there is very good agreement between our model and the data. Data from multiple shots in both Xe and He are presented (see Table 1). The values shown here represent a mean deceleration between 0 and ~ 10 ns. This allows us to validate our model, which reproduces the observed experimental deceleration for different initial shock velocities. The initial Mihalas number is also given as a simple measure of the expected importance of radiative effects, as well as the shock temperature (eV). According to the FCI2 code, the temperature values are expected to have less than $\pm 5\%$ errors bars, leading to a $\pm 15\%$ error in R .

We also note that Equation (4) shows indirectly that the system described above can be hydrodynamically unstable. Since the acceleration is opposed to the density gradient, the Rayleigh–Taylor (RT) instability is of particular interest. The growth rate of this instability can be expressed as $\gamma = \sqrt{Agk}$ where A is the Atwood number, g the absolute acceleration of the shock front, and k the spatial wavenumber. Taking typical laboratory values of $A = 1$, $g = 4 \text{ km s}^{-1} \text{ ns}^{-1}$, and $k = 2\pi/250 \mu\text{m}^{-1}$ (as $250 \mu\text{m}^{-1}$ is the typical shock radius) gives us a characteristic time of 6.4 ns. This value is similar to the characteristic experiment timescale and the deceleration

Table 1
Analysis of Six Shots for Various Initial Velocities u_0

Gas	u_0 (km s^{-1})	$a_{0,\text{exp}}$	$a_{0,\text{th}}$	$a_{0,\text{sim}}$	R_0	T_s (eV)
Xe 31 mbar	165	6.2 ± 2.1	6.1	5.1	9	24.4
He 1 bar	145	-0.4 ± 1.8	0	0.4	102	64.8
Xe 31 mbar	122	3.4 ± 1.2	3.1	2.3	15	19.4
He 1 bar	120	0.1 ± 1.2	0	0.3	230	49
Xe 31 mbar	107	2.0 ± 1.3	1.4	1.6	65	17.6
He 1 bar	114	0.6 ± 1.2	0	0.3	660	44.6

Note. $a_{0,\text{exp}}$, $a_{0,\text{th}}$, and $a_{0,\text{sim}}$ are the experimental, theoretically modeled, and numerically simulated shock deceleration (in $\text{km s}^{-1} \text{ ns}^{-1}$) respectively.

time that appears in Equation (4). Future experiments may therefore be able to study the evolution of this process.

6. Astrophysical Implication

Turning to the astrophysical case, we take as an example SN 1987A, where the expanding debris struck a dense circumstellar equatorial ring (ER), one of three already present before the supernova explosion, leading to the observation of various hotspots. The reason for the presence of these rings is unclear but they may be attributed to interacting stellar winds (Sugerman et al. 2005). This allows us to determine the characteristic length of the disturbance, which is typically the distance between two hotspots in the ER. As the shock passes, the initial disturbance becomes amplified as the radiatively decelerating shock front is RT-unstable. Using our analytical solution, one is able to determine the characteristic time of the dynamics of the amplification of the initial disturbance.

In greater detail, the initial collision created an RS at a velocity of 250 km s^{-1} in a dense ($n \approx 3.3 \times 10^4 \text{ cm}^{-3}$) medium (Pun et al. 2002). Significantly, the ring is optically thick to radiation coming from the shock. Indeed, the Rosseland mean free path in the ER is $\lambda_R \approx 5 \times 10^{15} \text{ m}$ (calculated under the Thomson scattering hypothesis). The shock transmitted in the gas is radiative and has a radiative precursor length of $\approx 3 \times 10^{14} \text{ m}$ (Pun et al. 2002). For $R_0 + 1 \approx 1$, this gives a characteristic deceleration time of $t_c \approx 15$ days, which is less than the time taken for the shock to traverse the ER, ≈ 10 yr. We can therefore expect the shock to radiatively decelerate as it propagates. Previous astrophysical studies, however, have assumed a constant shock velocity and ignored the effects of optical thickness and radiative precursors (Sugerman et al. 2002), instead relying on the approach using a cooling function as discussed previously. As in the laboratory case, radiative deceleration can lead to RT instabilities. Taking the initial deceleration as predicted by Equation (4), the characteristic time for the RT growth is given by

$$t_{\text{RT}} = \sqrt{\frac{6t_c}{kAu_0}}, \quad (5)$$

giving $t_{\text{RT}} \sim 250$ days for the case of SN 1987A. This timescale is shorter than typical calculated cooling times in this system (several years) (Pun et al. 2002) and, crucially, is similar to the timescale over which the hotspots evolve (Sugerman et al. 2002; Fransson et al. 2015). Although a detailed model of this system is far beyond the scope of this

work, these calculations show that this mechanism may play a role in the formation and evolution of hotspots in SN 1987A.

7. Summary

In conclusion, RS deceleration in an optically thick medium is observed in the laboratory for the first time. An analytical model is developed in order to explain this deceleration and is consistent with experimental and numerical results. The model is extended to the case of SN 1987A, where ejecta from the supernova generate a shock in a dense circumstellar ER, showing that the shock transmitted is expected to undergo significant radiative deceleration. The system is therefore unstable to the RT instability, with a growth time similar to the timescale of the evolution of the system. In addition to the cooling instability (Chevalier et al. 1992), this mechanism may therefore contribute to the formation of the observed hotspots.

This work was performed under the joint research project of the Institute of Laser Engineering, Osaka University. The authors would like to thank the ILE staff for their great support. This work received funding from Investments d’Avenir of PALM Labex (ANR-10-LABX-0039-PALM). We also acknowledge the work done by the GEPI target fabrication team. This work was partially supported by JSPS KAKENHI grant Nos.17H06202 and by the Osaka University’s International Joint Research Promotion Program.

ORCID iDs

T. Sano  <https://orcid.org/0000-0001-9106-3856>

References

- Bouquet, S., Stéhlé, C., Koenig, M., et al. 2011, *PhRvL*, **92**, 225001
 Busschaert, C., Falize, É., Michaut, C., et al. 2015, *A&A*, **579**, A25
 Chevalier, R. A. 1982, *ApJ*, **258**, 790
 Chevalier, R. A., Blonding, J. M., Emmering, R. T., et al. 1992, *ApJ*, **392**, 118
 Doss, F. W., Robey, H. F., Drake, R. P., & Kuranz, C. C. 2009, *PhPI*, **16**, 112705
 Drake, R. P. 2005, *Ap&SS*, **298**, 49
 Drake, R. P. 2007, *PhPI*, **14**, 043301
 Drake, R. P., Doss, F. W., McClarren, R. G., et al. 2011, *HEDP*, **7**, 130
 Edwards, M. J., MacKinnon, A. J., Zweiback, J., et al. 2001, *PhRvL*, **87**, 085004
 Ensmann, L., & Burrows, A. 1992, *ApJ*, **393**, 742
 Fransson, C., Larsson, J., Migotto, K., et al. 2015, *ApJL*, **806**, L19
 Hansen, J. F., Edwards, M. J., Froula, D. H., et al. 2006, *PhPI*, **13**, 022105
 Hohenberger, M., Symes, D. R., Lazarus, J., et al. 2010, *PhRvL*, **105**, 205003
 Koenig, M., Michel, Th., Yurchak, R., et al. 2017, *PhPI*, **24**, 082707
 Lawrence, S. S., Sugerman, B. E., Bouchet, P., et al. 2000, *ApJL*, **537**, L123
 Michaut, C., Falize, E., Cavet, C., et al. 2009, *Ap&SS*, **322**, 77
 Michel, Th., Falize, E., Albertazzi, B., et al. 2018, *High Power Laser Sci. Engineer.*, **6**, e30
 Müller, E., Fryxell, B., & Arnett, D. 1991, *A&A*, **251**, 505
 Nagakura, T., Hosokawa, T., Omukai, K., et al. 2009, *MNRAS*, **399**, 2183
 Orlando, S., Bonito, R., Argiroffi, C., et al. 2013, *A&A*, **559**, A127
 Orlando, S., Miceli, M., Pumo, M. L., & Bocchino, F. 2015, *ApJ*, **810**, 168
 Pun, C. S. J., Michael, E., Zhekov, S. A., et al. 2002, *ApJ*, **572**, 906
 Schurtz, G. P., Nicolai, P. D., Busquet, M., et al. 2000, *PhPI*, **7**, 4238
 Shapiro, S. L., & Salpeter, E. E. 1975, *ApJ*, **198**, 671
 Staveley-Smith, L., Briggs, D. S., Rowe, A. C. H., et al. 1993, *Natur*, **366**, 136
 Sugerman, B. E., Crotts, A. P. S., Kunkel, W. E., Heathcote, S. R., & Lawrence, S. S. 2005, *ApJS*, **159**, 60
 Sugerman, B. E., Lawrence, S. S., Crotts, A. P. S., Bouchet, P., & Heathcote, S. R. 2002, *ApJ*, **572**, 209
 Suzuki-Vidal, F., Clayson, T., Stéhlé, C., et al. 2011, *PhRvL*, **119**, 055001
 Van Box Som, L., Falize, E., Bonnet-Bidaud, J.-M., et al. 2018, *MNRAS*, **473**, 3158
 Vinci, T., Koenig, M., Benuzzi-Mounaix, A., et al. 2006, *PhPI*, **13**, 010702
 Zel’dovich, I. A. B., & Raizer, Y. P. 2002, *Physics of Shock Waves and High-Temperature Hydrodynamic Phenomena* (New York: Dover)